International Journal of Multiphase Flow 35 (2009) 896–903

Contents lists available at ScienceDirect

International Journal of Multiphase Flow

journal homepage: www.elsevier.com/locate/ijmulflow

Measurement of liquid film thickness in micro square channel

Youngbae Han *, Naoki Shikazono

Department of Mechanical Engineering, The University of Tokyo, Hongo 7-3-1, Bunkyo-ku, Tokyo 113-8656, Japan

ARTICLE INFO

Article history:
Received 14 April 2009
Received in revised form 17 June 2009
Accepted 23 June 2009
Available online 2 July 2009

Keywords:
Slug flow
Liquid film thickness
Micro channel

ABSTRACT

In micro channels, slug flow becomes one of the main flow regimes due to strong surface tension. In micro channel slug flow, elongated bubble flows with the thin liquid film confined between the bubble and the channel wall. Liquid film thickness is an important parameter in many applications, e.g., micro heat exchanger, micro reactor, coating process etc. In the present study, liquid film thickness in micro square channels is measured locally and instantaneously with the confocal method. Square channels with hydraulic diameter of D_h = 0.3, 0.5 and 1.0 mm are used. In order to investigate the effect of inertial force on the liquid film thickness, three working fluids, ethanol, water and FC-40 are used. At small capillary numbers, liquid film at the channel center becomes very thin and the bubble interface is not axisymmetric. However, as capillary number increases, bubble interface becomes axisymmetric. Transition from non-axisymmetric to axisymmetric flow pattern starts from lower capillary number as Reynolds number increases. An empirical correlation for predicting axisymmetric bubble radius based on capillary number and Weber number is proposed from the present experimental data.

1. Introduction

Flow boiling in micro channels has been studied extensively, since heat transfer is enhanced effectively in micro scales. It is known that the flow boiling characteristics of micro channels are quite different from those found in conventional channels. In micro channels, vapor bubble growth is restricted by the channel wall, and elongated vapor bubbles are confined by liquid slugs and liquid film. This flow regime is called slug flow. It is reported that the liquid film thickness is one of the important parameters for predicting boiling heat transfer in micro channel slug flows (Thome et al., 2004; Kenning et al., 2006; Serin et al., 2008).

For the pioneer study, Fairbrother and Stubbs (1935) investigated the bubble velocity in a circular tube. They reported that the bubble velocity is faster than the liquid slug velocity due to the liquid film attached to the tube wall. An experimental correlation for the bubble velocity was proposed as follows:

$$(U_b - U_m)/U_m = 1.0Ca^{1/2}, \quad (1)$$

where U_b and U_m are the bubble velocity and the mean velocity, respectively. Taylor (1961) extended Fairbrother and Stubbs' experiment to higher capillary numbers. It was observed that the ratio of bubble velocity and mean velocity approaches an asymptotic value around 0.55. Bretherton (1961) proposed a theoretical correlation for the liquid film thickness with the lubrication equations as follows:

$$\delta/D = 0.67Ca^{2/3}, \quad (2)$$

where δ is the liquid film thickness and D is the tube diameter. However, Eq. (2) is applicable only for small capillary number flows. Ratulowski and Chang (1989) extended Bretherton's theory to higher capillary number with arclength-angle formulation. It was shown that film thickness and pressure drop of the flow with finite bubble length resembles those of the flow with an infinitely long bubble when bubble length exceeds channel width.

Aussillous and Quere (2000) measured the averaged liquid film thickness from the length variation of the liquid slug with low viscosity fluids. It was found that the liquid film thickness is thicker than the Taylor's experimental data at high capillary numbers due to the inertial effect. Han and Shikazono (2009) measured the initial liquid film thickness in micro circular tubes with laser focus displacement meter. The effect of inertia force was investigated using different working fluids and different diameter tubes. An empirical correlation based on capillary number, Reynolds number and Weber number was proposed.

Numerical studies on the liquid film thickness have also been conducted. Giavedoni and Saita (1997) used finite-element method to investigate the motion of a bubble confined either between two closely separated plates or in a small cylindrical tube. Heil (2001) investigated the effect of Reynolds number on the flow field and pressure distribution in micro tube slug flow. It is reported that the liquid film thickness decreases initially with Reynolds number,

* Corresponding author. Tel.: +81 3 5841 6419; fax: +81 3 5800 6999.
E-mail addresses: ybhan@feslab.t.u-tokyo.ac.jp (Y. Han), shika@feslab.t.u-tokyo.ac.jp (N. Shikazono).

0301-9322/$ - see front matter © 2009 Elsevier Ltd. All rights reserved.
doi:10.1016/j.ijmultiphaseflow.2009.06.006

and this tendency is reversed as Reynolds number increases. Kreutzer et al. (2005) showed that the pressure drop increases significantly as inertial force becomes dominant. The effect of Reynolds number on the liquid film thickness was similar to the numerical results of Heil (2001).

Compared with the circular tube studies, researches on the square channel two-phase flows are still limited. In square channels, liquid film thickness varies along the channel perimeter. Theoretical approach of the two-phase flow becomes more complicated due to the presence of channel corner. Wong et al. (1995a, b) studied the liquid film deposited on polygonal capillaries at $Ca \rightarrow 0$ limit, and calculated the drag of the bubble. It was found that the deposited film is not uniform in the cross-stream direction and rearranges downstream. Kolb and Cerro (1991) used sequential particle tracking techniques to investigate the coating thickness of the liquid deposited on the square channel wall. It is observed that the transition from a non-axisymmetric to axisymmetric bubble occurs at $Ca \approx 0.1$. In their investigation, air–liquid interface consists of three regions: (1) a cap region defined by a circular sector of constant radius, (2) a transition region with its interface having a small slope, (3) a liquid film region with uniform thickness. Thulasidas et al. (1995, 1997) investigated the slug flow in capillary square channel with the same method as Kolb and Cerro (1991). They observed that the transition from non-axisymmetric to axisymmetric bubble occurs at $Ca \approx 0.04$.

Hazel and Heil (2002) numerically investigated the propagation of air-finger into elliptical and rectangular channels. It was observed that the liquid tends to move towards the corner due to the non-uniform pressure distribution at small capillary number. They found that the decay rate of the tip asymmetry decreases as capillary number increases. Taha and Cui, 2006 used VOF method to study the characteristics of slug flow in circular tubes and square channels. Bubble shape, velocity and wall shear stress distributions were investigated for the wide range of capillary number.

Hydrodynamics of square channel slug flows are thus quite different from those of circular tubes. Therefore, to develop a precise model of flow boiling in micro square channels, it is important to measure the instantaneous variation of the local liquid film thickness. In the present study, local and instantaneous liquid film thicknesses in micro square channels are measured directly with the confocal method which is used in the previous study (Han and Shikazono, 2009). Series of experiments is conducted to investigate the parameters that affect the liquid film thickness in micro square channels.

2. Experimental setup and procedures

2.1. Test section configuration

Square quartz channels (Conic Techno©) with hydraulic diameters of $D_h = 0.3$, 0.5 and 1.0 mm are used in the present study. Fig. 1 shows the cross section of the $D_h = 1.0$ mm square channel. In square channels, there are two representative liquid film thicknesses, i.e., liquid film thickness at the channel center δ_{center} and that at the channel corner δ_{corner}. The shapes of the channel corners are modified to measure the liquid film thickness at the channel corner as shown in Fig. 1. In order to investigate the effect of corner shape, the shapes of four corners of $D_h = 1.0$ mm square channel are modified differently. The channel is not a perfect square and the channel side is slightly curved. Circumscribed square can be drawn as shown in Fig. 2. Each corner and channel side is numbered and the distances between the corners of circumscribed and real squares are measured as shown in Fig. 2. Hydraulic diameters of the circumscribed squares are used for the data reduction.

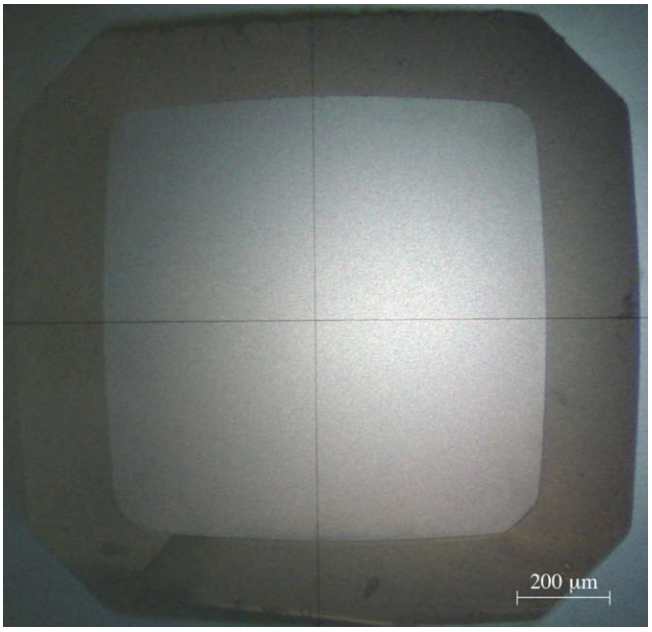

Fig. 1. Cross section of $D_h = 1.0$ mm square channel.

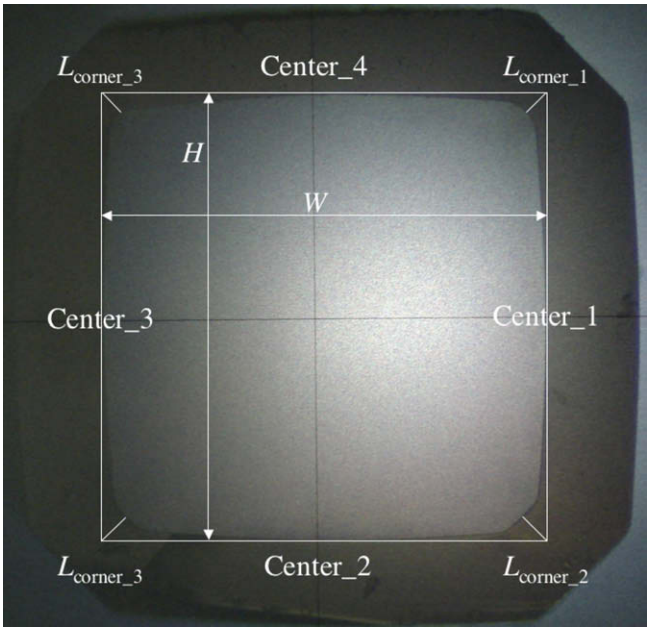

Fig. 2. Circumscribed square of $D_h = 1.0$ mm square channel.

Fig. 3(a–d) shows the cross sections and circumscribed squares of $D_h = 0.3$ and 0.5 mm square channels, respectively. For $D_h = 0.3$ and 0.5 mm channels, only one of the four corners is modified. Table 1 shows the dimensions of the micro square channels used in the present study.

2.2. Experimental setup and procedures

Experimental setup is the same as the previous study (Han and Shikazono, 2009). Fig. 4 shows the schematic diagram of the experimental setup. Actuator motor (EZHC6A-101, Oriental motor) is used to move the liquid in the micro channel. The images of interface movement are captured with high-speed camera (Phantom 7.1), and liquid film thickness is measured with laser focus dis-

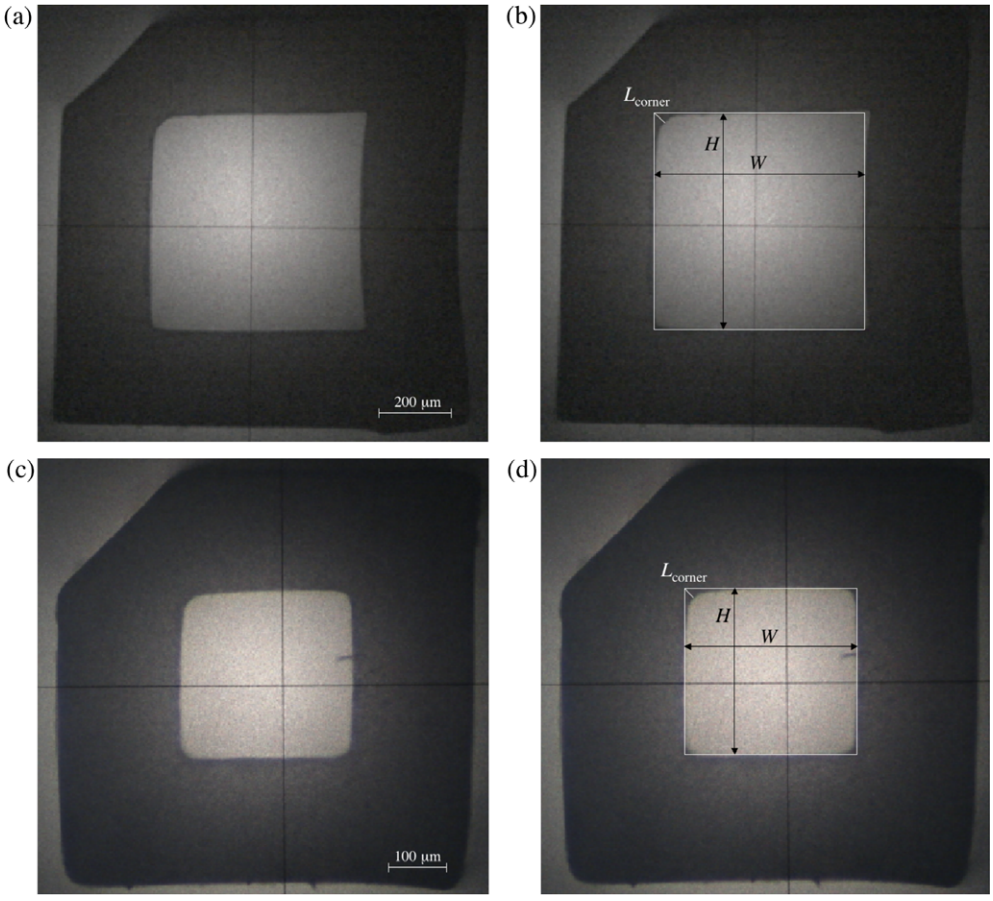

Fig. 3. Cross sections and circumscribed squares of square channels: (a) and (b) D_h = 0.5 mm square channel, (c) and (d) D_h = 0.3 mm square channel.

Table 1
Dimensions of micro square channels.

D_h (μm)	H (μm)	W (μm)	L_{corner_1} (μm)	L_{corner_2} (μm)	L_{corner_3} (μm)	L_{corner_4} (μm)
954.5	956	953	61.6	74.8	72.7	58.5
569.7	582	558		34.6		
281.5	279	284		20.3		

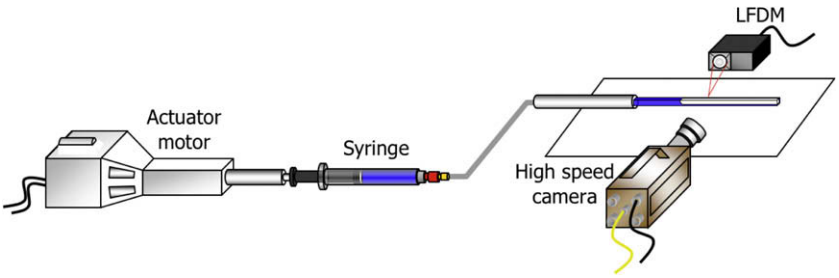

Fig. 4. Schematic diagram of the experimental setup.

placement meter (hereafter LFDM; LT9010M, Keyence). Three working fluids, water, ethanol and FC-40 are used to investigate the effect of property difference on the liquid film thickness. The principle and detailed specification of the present experiment are explained in the previous paper (Han and Shikazono, 2009).

Fig. 5 shows the path of laser through the channel wall and the liquid film. Refractive indices of quartz, ethanol, water and FC-40 are 1.457, 1.36, 1.33 and 1.29, respectively. Wall thickness y_1 is measured initially without flowing the liquid, and then the distance from outer wall to air–liquid interface y_2 is measured. Liquid film thickness δ_f is calculated from the difference of these two values:

$$\delta_f = (y_2 - y_1)\tan\theta_{air}/\tan\theta_f, \quad (3)$$

where θ_{air} and θ_f are the angle of incidence for air and liquid film. The angle of incidence θ_{air} for the present LFDM is 14.91°. The angle of incidence θ_f is obtained from the Snellius' law as follows:

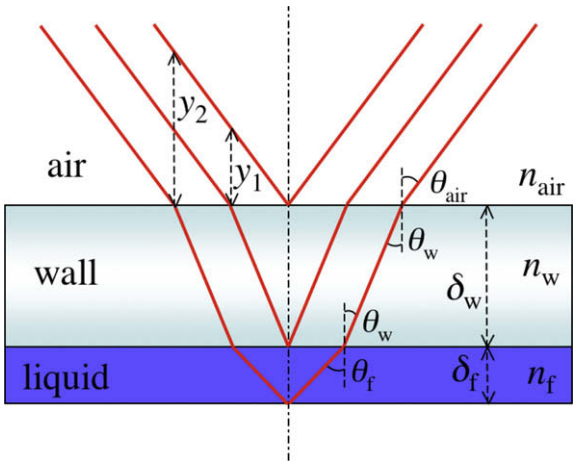

Fig. 5. Laser paths in channel wall and liquid film.

$$\theta_f = a\sin\left(\sin\theta_w \frac{n_w}{n_f}\right), \quad (4)$$

$$\theta_w = a\sin\left(\sin\theta_{air} \frac{n_{air}}{n_w}\right), \quad (5)$$

where n_{air}, n_w and n_f are the refractive indices of air, channel wall and fluid, respectively. Liquid film thickness δ_f is calculated from Eqs. (3)–(5).

3. Results and discussion

3.1. Time variation of the liquid film thickness

Fig. 6 shows a typical measurement data of ethanol in D_h = 1.0 mm channel at low capillary number, Ca = 0.011. In Fig. 6, a circular tube data δ_{tube} is also shown for comparison. Liquid film thickness in a circular tube becomes nearly constant after the initial rapid decrease, which corresponds to the transition region between bubble nose and flat film region. Liquid film thickness at the channel center is much thinner than that in the circular tube.

Fig. 7 shows the time variations of δ_{corner} and δ_{center}. Channel center thickness continues to decrease with wavy fluctuations. Frequency of the fluctuation also decreases with time. On the contrary, liquid film thickness at the channel corner tends to increase after the initial decrease and then approaches an asymptotic value. It is considered that the deposited liquid film flows from channel center to channel corner due to the pressure gradient along the channel perimeter. This secondary flow is also reported in the numerical work conducted by Hazel and Heil (2002). Asymptotic values after this secondary flow have terminated are defined as initial liquid film thicknesses. For fluctuating cases, the lower value is taken as shown in Fig. 7.

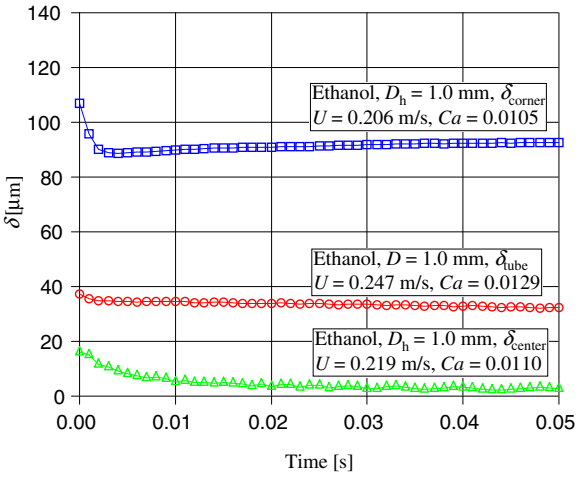

Fig. 6. Variation of liquid film thickness with time at low capillary number.

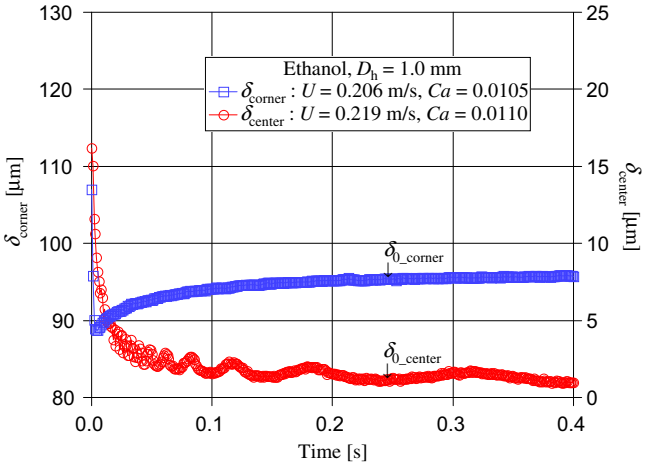

Fig. 7. Long time variation of δ_{corner} and δ_{center} at low capillary number in ethanol/air experiment.

Figs. 8 and 9 show the time variations of δ_{corner} and δ_{center} in FC-40/air and water/air experiments. The trend in FC-40/air experiment is almost the same as the ethanol/air experiment because FC-40 also wets quartz well. On the contrary, quartz wall becomes partially dry at the channel center for water/air experiment, because water does not wet quartz wall. The liquid film keeps its initial shape for a very short period and then liquid droplet is formed and the quartz wall becomes partially dry. Data just before the channel wall to become dry is used for δ_{0_center} as shown in Fig. 9.

Fig. 10 shows a typical measurement data of ethanol in D_h = 1.0 mm square channel at high capillary number, Ca = 0.063. Again, liquid film thickness at channel center is much thinner than that in a micro circular tube. Unlike the case of low capillary number, no fluctuation is observed. This trend was almost the same for

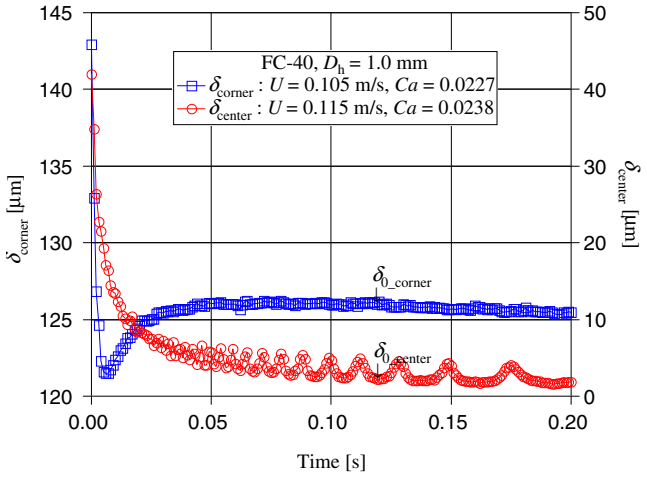

Fig. 8. Long time variation of δ_{corner} and δ_{center} at low capillary number in FC-40/air experiment.

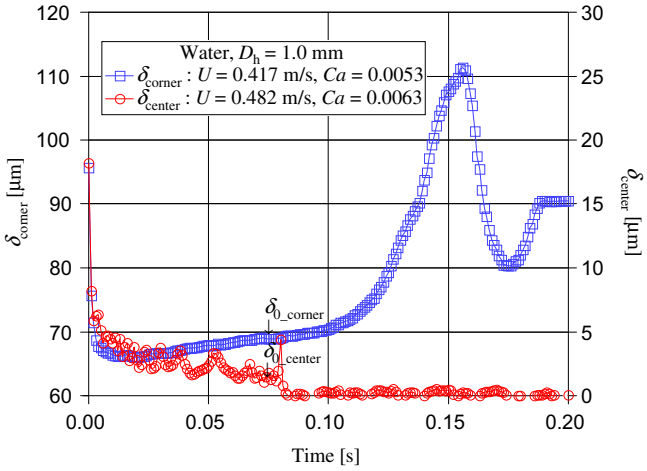

Fig. 9. Long time variation of δ_{corner} and δ_{center} at low capillary number in water/air experiment.

other fluids. The values after the initial decrease are used for the initial liquid film thicknesses as shown in Fig. 10.

3.2. Effect of modified corner shape

The effect of the modified corner shapes on the liquid film thickness is investigated. Fig. 11 shows the liquid film thicknesses at four corners of the D_h = 1.0 mm channel. Liquid film thickness at channel center is almost identical to each other. It is confirmed that the modified corners have no effect on the liquid film thickness at channel center. On the other hand, liquid film thicknesses at different channel corners show slight variations. In Fig. 12, δ_{0_corner} which are defined as the distances from air–liquid interface to circumscribed square corners are shown. Liquid film thicknesses defined from the circumscribed square corners are almost identical. Thus, the effect of modified corner shapes on the air–liquid interface profile is negligible if circumscribed square is used. Thus, in the following sections, distance from circumscribed square corner to the air–liquid interface is used for δ_{0_corner}.

Dimensionless bubble radii R_{center} and R_{corner} are commonly used in square channels:

$$R_{center} = 1 - \frac{2\delta_{0\_center}}{D_h}, \tag{6}$$

$$R_{corner} = \sqrt{2} - \frac{2\delta_{0\_corner}}{D_h}. \tag{7}$$

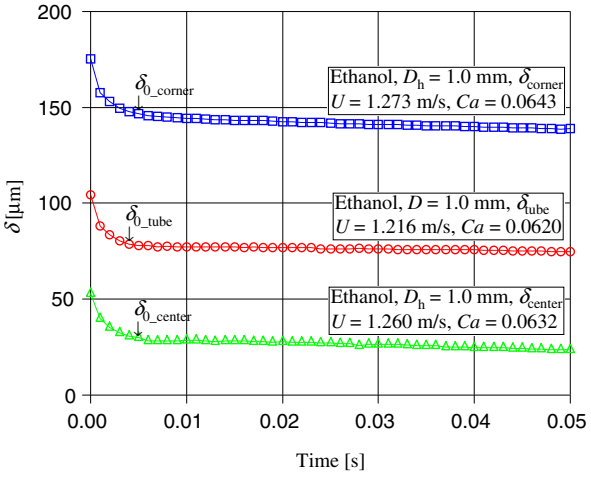

Fig. 10. Variation of liquid film thickness with time at high capillary number.

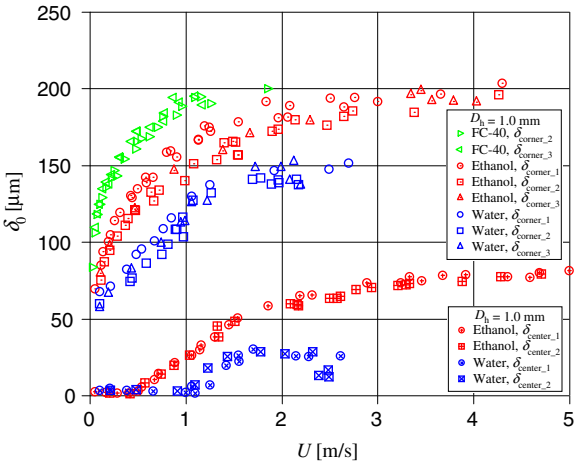

Fig. 11. Liquid film thickness against velocity in D_h = 1.0 mm square channel.

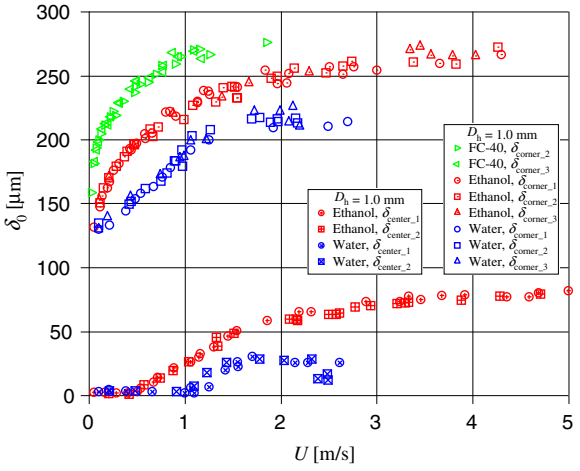

Fig. 12. Distance from the air–liquid interface to the ideal corner in D_h = 1.0 mm square channel.

When the liquid film thickness at the channel center δ_{0_center} is zero, R_{center} becomes unity. If the interface shape is axisymmetric, R_{center} becomes identical to R_{corner}.

3.3. FC-40/air experiment

Fig. 13 shows R_{center} and R_{corner} against capillary number for the FC-40/air experiment. The solid lines in Fig. 13 are the numerical simulation results obtained by Hazel and Heil (2002). In their simulation, inertial force term was neglected and thus it can be considered as the low Reynolds number limit. R_{center} is almost unity at capillary number less than 0.03. Corner radius R_{corner} monotonously decreases as capillary number increases. Thus, interface shape is non-axisymmetric for $Ca < 0.03$.

For $Ca > 0.03$, R_{center} becomes nearly identical to R_{corner} and the interface shape becomes axisymmetric. In Fig. 13, the bubble radii in D_h = 0.3 and 0.5 mm channels are almost identical and larger than the numerical simulation results. On the other hand, the bubble radius in D_h = 1.0 mm channel is smaller than those of the D_h = 0.3 and 0.5 mm channels for the whole capillary number range.

As capillary number approaches zero, liquid film thickness in a micro circular tube becomes zero. In micro square channels, even as capillary number approaches zero, liquid film δ_{0_corner} still

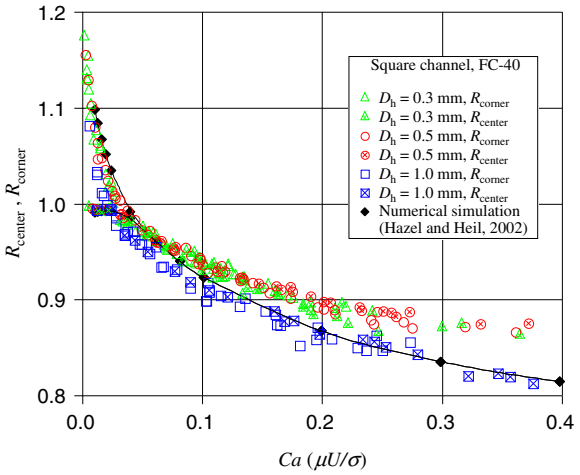

Fig. 13. Dimensionless bubble diameter against capillary number for the FC-40/air experiment.

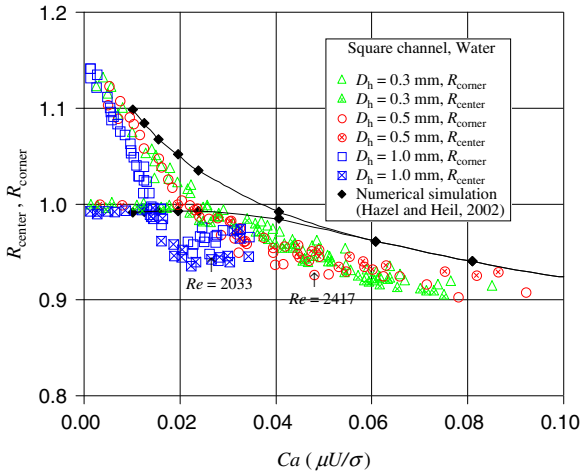

Fig. 15. Dimensionless bubble diameter against capillary number for the water/air experiment.

remains at the channel corner. Corner radius R_{corner} reaches an asymptotic value smaller than $\sqrt{2}$ as investigated in Wong et al.'s numerical study (1995a,b). It is reported that liquid film thickness at the channel corner takes a certain value under stationary condition (Wong et al., 1995a,b).

3.4. Ethanol/air experiment

Fig. 14 shows R_{center} and R_{corner} against capillary number for the ethanol/air experiment. Similar to the trend found in the FC-40/air experiment, R_{center} is almost unity at low capillary number. Most of the experimental data are smaller than the numerical results. Transition capillary number, which is defined as the capillary number when bubble shape changes from non-axisymmetric to axisymmetric, becomes smaller as D_h increases. For D_h = 1.0 mm square channel, R_{center} is almost identical to R_{corner} beyond the transition capillary number. But for D_h = 0.3 and 0.5 mm channels, R_{center} is smaller than R_{corner} even at large capillary numbers. At the same capillary number, R_{center} and R_{corner} decrease as Reynolds number increases.

For Ca > 0.17, R_{center} and R_{corner} in D_h = 1.0 mm square channel becomes nearly constant. It is considered that this different trend is attributed to the flow transition from laminar to turbulent. At

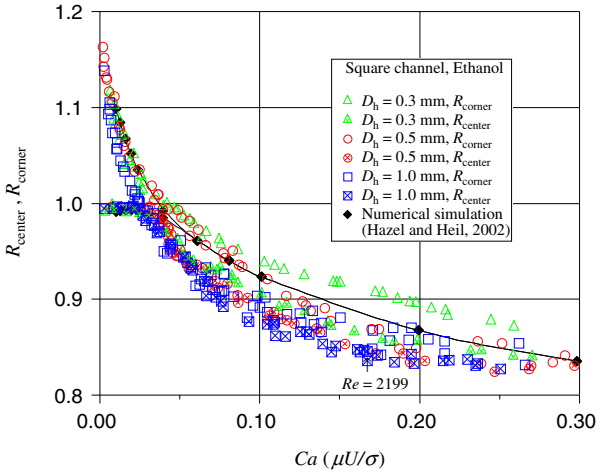

Fig. 14. Dimensionless bubble diameter against capillary number for the ethanol/air experiment.

$Ca \approx 0.17$, Reynolds number $Re = \rho U D_h/\mu$ of ethanol in D_h = 1.0 mm channel becomes nearly 2000 as indicated in Fig. 14.

3.5. Water/air experiment

Fig. 15 shows R_{center} and R_{corner} against capillary number for the water/air experiment. R_{center} is again almost unity at low capillary number. Transition capillary number is much smaller than those of ethanol/air and FC-40/air experiments. Transition capillary numbers for D_h = 0.3, 0.5 and 1.0 mm square channels are Ca = 0.025, 0.2 and 0.014, respectively. Due to the strong inertial effect, bubble diameter of the water/air experiment is much smaller than those of other fluids and the numerical results. Bubble diameter becomes nearly constant again for Re > 2000. Data points at $Re \approx 2000$ are indicated in Fig. 15. Inertial effect is usually neglected in micro scales. However, it is apparent that inertial effect must be considered even for this Reynolds number range.

3.6. Scaling analysis and experimental correlation

Fig. 16 shows the schematic diagram of the force balance in the transition region. Momentum equation and curvature matching in the transition region are expressed as follows:

$$\frac{\mu U}{\delta^2} \sim \frac{1}{\lambda}\sigma(\kappa_1 - \kappa_2) - \frac{1}{\lambda}\rho U^2, \tag{8}$$

$$\frac{\delta}{\lambda^2} \sim \kappa_1 - \kappa_2, \tag{9}$$

where λ is the length of transition region and κ_1 and κ_2 are the curvatures of bubble nose and flat film region, respectively.

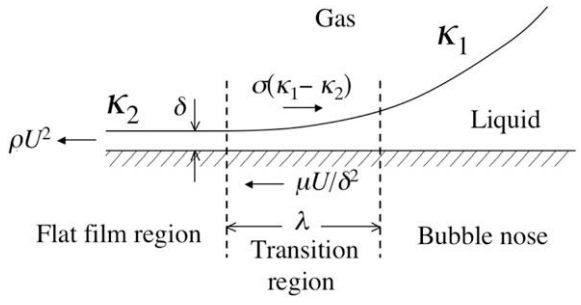

Fig. 16. Schematic diagram of the force balance in the transition region.

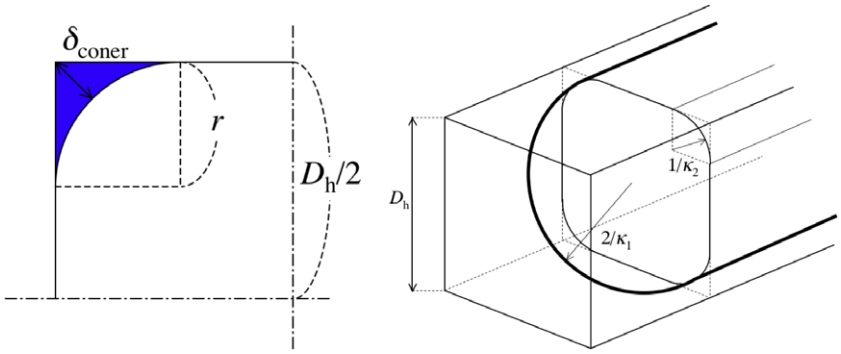

Fig. 17. Schematic diagram of the interface shape at $Ca \to 0$.

In the present experiment, δ_{0_corner} does not become zero but takes a certain value as $Ca \to 0$. Fig. 17 shows the schematic diagram of the interface shape at $Ca \to 0$. In Fig. 17, air–liquid interface is assumed as an arc with radius r, and thus κ_2 can be expressed as follows:

$$\kappa_2 = \frac{1}{r} = \frac{\sqrt{2}-1}{\delta_{0\_corner}}. \tag{10}$$

If bubble nose is assumed to be a hemisphere of radius $D_h/2$, the curvature of bubble nose κ_1 can be expressed as follows:

$$\kappa_1 = \frac{2}{D_h/2}, \tag{11}$$

The curvature of bubble nose κ_1 should be larger than the curvature of the flat film region κ_2 due to the momentum balance. Then, the relation of D_h and δ_{0_corner} from the restraint $\kappa_2 \leqslant \kappa_1$ is deduced as follows:

$$\frac{\sqrt{2}-1}{\delta_{0\_corner}} \leq \frac{2}{D_h/2}, \tag{12}$$

From Eq. (12), the limit of R_{corner} is determined as follows:

$$R_{corner} \leq 1.171. \tag{13}$$

Fig. 18 is a magnification of R_{corner} at small capillary number range. As capillary number approaches zero, R_{corner} reaches 1.171. This implies that $\kappa_1 = \kappa_2$ is a good estimation at $Ca \to 0$.

As capillary number increases, the interface shape becomes axisymmetric for most of the experimental conditions. Thus, bubble can be simply assumed to be a hemisphere at bubble nose and $R_{corner} = R_{center}$ at flat film region. Under such assumption, the curvatures κ_1 and κ_2 in Eqs. (8) and (9) can be rewritten as follows:

$$\kappa_1 = \frac{2}{D_h/\sqrt{2} - \delta_{0\_corner}}, \tag{14}$$

$$\kappa_2 = \frac{1}{D_h/\sqrt{2} - \delta_{0\_corner}}, \tag{15}$$

$$\kappa_1 - \kappa_2 = \frac{1}{D_h/\sqrt{2} - \delta_{0\_corner}}. \tag{16}$$

We can deduce a relation for δ_{0_orner}/D_h from Eqs. (8), (9) and (16) as follows:

$$\frac{\delta_{0\_corner}}{D_h} \sim \frac{\sqrt{2}Ca^{2/3}}{Ca^{2/3} + (1 - We')^{2/3}}, \tag{17}$$

where

$$We' = \frac{\rho U^2 (D_h/\sqrt{2} - \delta_{0\_corner})}{\sigma}. \tag{18}$$

We' includes δ_{0_corner} in the definition as shown in Eq. (18). Thus We' is replaced by $We = \rho U^2 D_h/\sigma$ for simplicity. The denominator of RHS in Eq. (17) is also simplified with Taylor expansion. From Eqs. (13) and (17), R_{corner} can be deduced as follows:

$$R_{corner} \sim 1.171 - \frac{2\sqrt{2}Ca^{2/3}}{1 + Ca^{2/3} - We'}. \tag{19}$$

The experimental correlation for R_{corner} is obtained by modifying the coefficients and exponents in Eq. (19) with the least linear square method as follows:

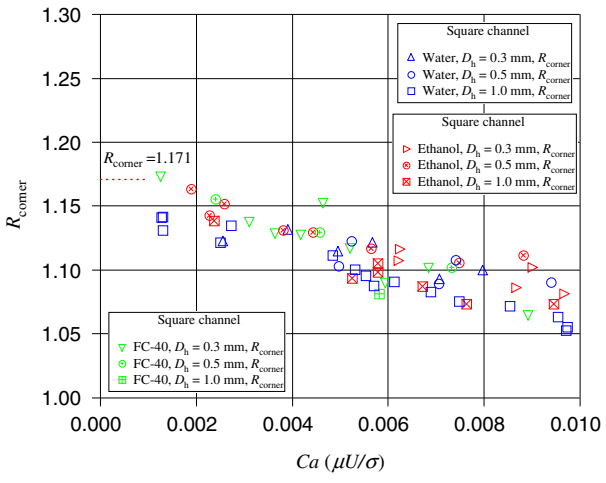

Fig. 18. Dimensionless bubble diameter R_{corner} against capillary number at $Ca \to 0$.

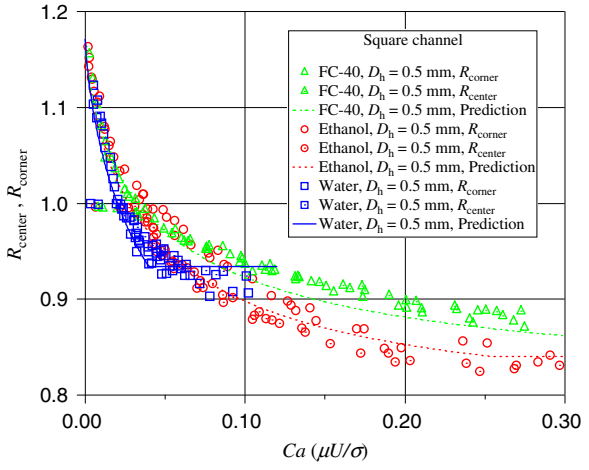

Fig. 19. Predicted bubble diameter against capillary number in $D_h = 0.5$ mm square channel.

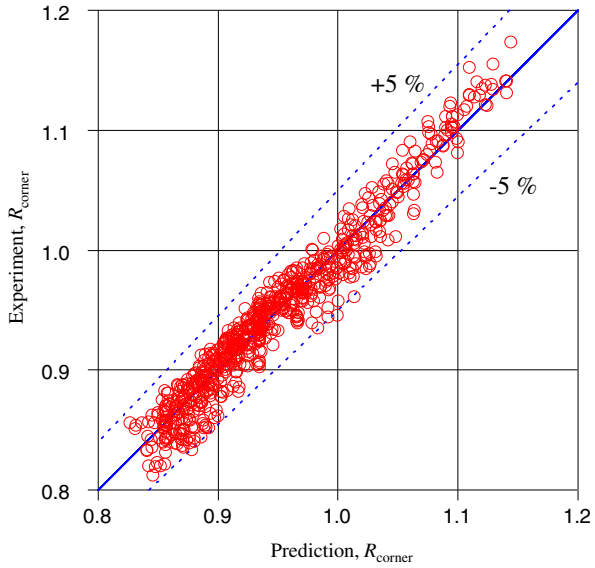

Fig. 20. Comparison between prediction and experimental results.

$$R_{corner} = \begin{cases} 1.171 - \frac{2.43Ca^{2/3}}{1+7.28Ca^{2/3}-0.255We^{0.215}} \\ \quad (Re < 2000)\ (a) \\ 1.171 - \frac{3869\mu^2/\rho\sigma D_h^{2/3}}{1+1.156(\mu^2/\rho\sigma D_h)^{2/3}-6.70(\mu^2/\rho\sigma D_h)^{0.215}} \\ \quad (Re \geq 2000)\ (b) \end{cases} \quad (20)$$

$$R_{center} \coloneqq \begin{cases} 1 & (R_{corner} > 1)\ (a) \\ R_{corner} & (R_{corner} \leq 1)\ (b) \end{cases} \quad (21)$$

where $Ca = \mu U/\sigma$, $Re = \rho U D_h/\mu$ and $We = \rho U^2 D_h/\sigma$. R_{center} is almost unity at small capillary number. However, δ_{0_center} still has a finite value at low Ca, thus $R_{center} \neq 1$. Further investigation is required for the accurate scaling of δ_{0_center} or R_{center} at low Ca. As capillary number increases, interface shape becomes axisymmetric and R_{center} is identical to R_{corner}. As capillary number approaches zero, R_{corner} should be a certain value as shown in Fig. 18 and the value is determined to be 1.171. If Reynolds number becomes larger than 2000, R_{corner} becomes constant due to the flow transition from laminar to turbulent. Capillary number and Weber number should be also replaced with the values at $Re = 2000$ as shown in Eq. (20b). Fig. 19 shows the comparison between the experimental data and the predictions of Eq. (20). As shown in Fig. 20, the present correlation can predict dimensionless bubble diameters within the range of ±5 % accuracy.

4. Concluding remarks

Liquid film thicknesses in micro square channels with hydraulic diameters of $D_h = 0.3$, 0.5 and 1.0 mm were measured with laser focus displacement meter. At small capillary numbers, it is observed that the liquid film formed on the channel center becomes very thin. However, as capillary number increases, the interface shape becomes axisymmetric. As Reynolds number increases, transition from non-axisymmetric to axisymmetric flow pattern starts from smaller capillary number. An empirical correlation for the dimensionless bubble diameter based on capillary number and Weber number is proposed. The present empirical correlation predicts the experimental data within ±5 % accuracy.

Acknowledgements

We thank Prof. Kasagi, Prof. Suzuki and Dr. Hasegawa for the fruitful discussions and suggestions. This work is supported through Grant in Aid for Scientific Research (No. 20560179) by MEXT, Japan.

References

Aussillous, P., Quere, D., 2000. Quick deposition of a fluid on the wall of a tube. Phys. Fluids 12, 2367–2371.
Bretherton, F.P., 1961. The motion of long bubbles in tubes. J. Fluid Mech. 10, 166–188.
Fairbrother, F., Stubbs, A.E., 1935. Studies in electroendosmosis – VI. The bubble tube method of measurement. J. Chem. Soc. 1, 527–529.
Giavedoni, M.D., Saita, F.A., 1997. The axisymmetric and plane cases of a gas phase steadily displacing a Newtonian liquid – a simultaneous solution of the governing equation. Phys. Fluids 9, 2420–2428.
Han, Y., Shikazono N. Measurement of the liquid film thickness in micro tube slug flow. Int. J. Heat Fluid Flow, accepted for publication.
Hazel, A.L., Heil, M., 2002. The steady propagation of a semi-infinite bubble into a tube of elliptical or rectangular cross-section. J. Fluid Mech. 470, 91–114.
Heil, M., 2001. Finite Reynolds number effects in the Bretherton problem. Phys. Fluids 13, 2517–2521.
Kenning, D.B.R., Wen, D.S., Das, K.S., Wilson, S.K., 2006. Confined growth of a vapour bubble in a capillary tube at initially uniform superheat: experiments and modeling. Int. J. Heat Mass Trans. 49, 4653–4671.
Kolb, W.B., Cerro, R.L., 1991. Coating the inside of a capillary of square cross section. Chem. Eng. Sci. 46, 2181–2195.
Kreutzer, M.T., Kapteijn, F., Moulijn, J.A., Kleijn, C.R., Heiszwolf, J.J., 2005. Inertial and interfacial effects on pressure drop of Taylor flow in capillaries. AIChE J. 51, 2428–2440.
Ratulowski, J., Chang, H.C., 1989. Transport of gas bubbles in capillaries. Phys. Fluids A 1, 1642–1655.
Serin, V., Mederic, B., Lavieille, P., Miscevic, M., 2008. Heat and mass transfer in capillary-pumped liquid films in square cross-section minichannels. Heat Transfer Eng. 29, 913–923.
Taha, T., Cui, Z.F., 2006. CFD modelling of slug flow inside square capillaries. Chem. Eng. Sci. 61, 665–675.
Taylor, G.I., 1961. Deposition of a viscous fluid on the wall of a tube. J. Fluid Mech. 10, 161–165.
Thome, J.R., Dupont, V., Jacobi, A.M., 2004. Heat transfer model for evaporation in micro channels. Part I: presentation of the model. Int. J. Heat Mass Trans. 47, 3375–3385.
Thulasidas, T.C., Abraham, M.A., Cerro, R.L., 1995. Bubble-train flow in capillaries of circular and square cross section. Chem. Eng. Sci. 50, 183–199.
Thulasidas, T.C., Abraham, M.A., Cerro, R.L., 1997. Flow patterns in liquid slugs during bubble-train flow inside capillaries. Chem. Eng. Sci. 52, 2947–2962.
Wong, H., Radke, C.J., Morris, S., 1995a. The motion of long bubbles in polygonal capillaries. Part 1. Thin films. J. Fluid Mech. 292, 71–94.
Wong, H., Radke, C.J., Morris, S., 1995b. The motion of long bubbles in polygonal capillaries. Part 2. Drag, fluid pressure and fluid flow. J. Fluid Mech. 292, 95–110.